Supporting Information

Electrochemical hydrogen evolution reaction efficiently catalyzed by Ru-N coupling in defect-rich Ru/g-C_3N_4 nanosheets

Dongze Li,[a] Yang Liu,[b] Zong Liu,[a] Jun Yang,[c] Chaoquan Hu,[c*] and Ligang Feng[a*]*

a School of Chemistry and Chemical Engineering, Yangzhou University, Yangzhou 225002, PR China. Email: liuzonglz@126.com (Z. Liu); ligang.feng@yzu.edu.cn; fenglg11@gmail.com (L Feng*); ORCID: 0000-0001-9879-0773 (L Feng)*

b School of Materials Science and Engineering, Henan Normal University, Xinxiang, Henan, 453007, P. R. China.

c State Key Laboratory of Multiphase Complex Systems, Institute of Process Engineering, Chinese Academy of Sciences, Beijing 100190, P. R. China.

Experimental section

Materials

All the reagents in the experiment were analytical grade and used as received. Ruthenium chloride hydrate ($RuCl_3 \cdot xH_2O$), ethylene glycol ($C_2H_6O_2$), and melamine ($C_3N_3(NH_2)_3$) were purchased from Shanghai Aladdin Bio-Chem Technology Co., LTD. Potassium hydroxide (KOH) and sulfuric acid (H_2SO_4) were purchased from Sinopharm Chemical Reagent Co., Ltd. Nafion (5 wt.%) was purchased from Sigma-Aldrich. Commercial Pt/C catalyst was purchased from Johnson Matthey Chemicals Ltd. All solutions were prepared with ultrapure water (Thermo Fisher Scientific (USA) Co., Ltd).

Catalysts fabrication

Synthesis of Ru/g-C_3N_4. A given amount of $RuCl_3$ aqueous solution (Ru: 20 mg/mL) and 1.2 g of melamine were dispersed in the ultrapure water (15 mL) and stirred for 30 min. Then the slurry was lyophilized with Freeze Dryer (Scientz-18N) and the grey-black precursor (Ru^{3+}/melamine) was obtained. The precursor was then transferred to a quartz tube with a thermal annealing temperature at 700°C under an N_2 atmosphere for 30 min. The as-prepared product was denoted as Ru/g-C_3N_4. For comparison and to deeply understand the interplay between the utilization efficiency of Ru and electrocatalytic activities of the Ru/g-C_3N_4 catalysts, several control samples were synthesized under identical conditions except that the amount of $RuCl_3$ aqueous solution was 0.05, 0.25 and 0.5 mL, respectively. The corresponding products were labeled as Ru/g-C_3N_4-1, Ru/g-C_3N_4-2 and Ru/g-C_3N_4-3, respectively. The g-C_3N_4 catalyst was synthesized following the same procedure without adding $RuCl_3$ aqueous solution.

Physical Characterizations

The samples were characterized on Bruker D8 advance X-ray diffraction (XRD) with Cu K_α radiation. The morphologies were examined with an FEI Sirion-200 scanning electron microscope (SEM) and a transmission electron microscope (TEM) operating at 200 kV. Energy-dispersive X-ray spectroscopy (EDS) images are obtained on a TECNAI G2 F30 transmission electron microscope (acceleration voltage: 300 kV). X-ray photoelectron spectroscopy (XPS) measurement is carried on an ECSALAB250Xi S3 spectrometer with an Al Kα radiation source. Raman scattering is performed on a Jasco Raman spectrometer with excitation by 532 nm laser light. Fourier transform infrared spectroscopy (FT-IR) data were collected using a Bruker Tensor 27 FTIR spectrometer. Thermo Gravimetric Analysis (TGA) was conducted using a TGA-FTIR A588 instrument.

Electrochemical measurements

All the chemical measurements were performed with a Bio-Logic VSP electrochemical workstation (Bio-Logic Co., France) and a conventional three-electrode system. The glassy carbon electrode (3 mm diameter, 0.07 cm^2) was

used as the working electrode; a saturated calomel electrode (SCE) and a Hg/HgO electrode were served as the reference electrode in acidic and alkaline solution, respectively; a graphite rod was chosen as the counter electrode. For HER measurements, the electrolyte solution (0.5 M H_2SO_4 and 1M KOH) was purged with N_2 (99.99%) for at least 10 min. 5 mg catalysts were dispersed in 1 mL solution containing 0.95 mL ethanol and 0.05 mL 5 wt.% Nafion with sonication for 30 min to form a homogeneous ink. All potentials were converted and referred to the reversible hydrogen electrode (RHE): E (RHE) = E (SCE) + 0.059 pH + 0.242 V, E (RHE) = E (Hg/HgO) + 0.059 pH + 0.098 V, and the ohmic potential drop was corrected using electrochemical impedance spectroscopy (EIS) methods according to the equation: $E_a = E_b - IR_s$, I is the corresponding current and R_s is the resistance of the system obtained from EIS plots (ca. 8-9 Ω), all data have been corrected for 90% iR potential drop. Polarization curves were recorded by linear sweep voltammetry (LSV) tests at a scan rate of 5 mV s^{-1}. The current density was obtained by normalizing the current to the geometric surface area of the glassy carbon electrode.

Tafel analysis

The overpotential values were defined by the Tafel equation: η=a+blog|j|, where η was the applied overpotential, j was the current density, then the Tafel slope (b) can be obtained.

ECSA measurements and calculations

The electrochemical active surface area can be calculated from the equation ECSA=C_{dl}/C_s on basis of the double-layer capacitance (C_{dl}), where the specific capacitance value was 40 μF cm^{-2}. To estimate the C_{dl}, we recorded the cyclic voltammograms in the non-faradaic potential region from 0.342 V-0.442 V vs. RHE in 0.5 M H_2SO_4 solution, from 0.245 to 0.345 V vs. RHE in 1 M KOH solution. The roughness factor (R_f) was calculated by R_f = ECSA/S, where S was generally equal to the geometric area of the electrode (in this work, S=0.07 cm^2).

Mass activity and Specific activity

The specific activity was obtained by normalizing the apparent current to ECSA. The mass activity was calculated by normalizing the apparent current to the quality of Ru based on EDS.

Turnover frequency (TOF)

Turn over frequency (TOF) values were calculated using the following equation by assuming Ru atoms in the HER: TOF (s^{-1}) = $I/(2*F*n)$, where I is the current (A) during linear sweep measurement, F is the Faraday's constant (96485.3 C/mol), n is the number of active sites (mol). The factor 1/2 is based on the consideration that two electrons are required to produce one hydrogen molecule.

Electrochemical Impendence Spectroscopy analysis

Electrochemical impedance spectroscopy (EIS) was recorded with a frequency range of 30 mHz-1000 kHz with an amplitude of 5 mV.

Stability test and Chronoamperometry measurements

The dynamical stability was tested for 10 000 cycles at the constant scan rate of 100 mV s^{-1}. After 10 000 cycles, the polarization curve was recorded for comparison with the initial curve. To estimate the stability of the catalysts, the chronoamperometry (CA) was also performed at a potential of -0.030 V and -0.035 V vs.RHE in 0.5 M H_2SO_4 and 1 M KOH solution, respectively.

Faradaic efficiency test

The working electrode was prepared by drop-casting catalyst suspension on the glassy carbon electrode with a surface area of 0.07 cm^{-2}. A constant potential was applied on the electrode and evolved gas was continually recorded, respectively. Thus, the faradaic efficiency was calculated from the ratio of $V_{experimental}$ (the recorded gas volume) to $V_{theoretical}$ (the theoretical gas volume) during the charge transport process.

The Faradic efficiency of HER was calculated with the following equation:

$$Faradaic\ efficiency = \frac{V_{experimental}}{V_{theoretical}} = \frac{V_{experimental}}{\frac{1}{2} \times \frac{Q}{F} \times V_m}$$

where Q is the total amount of charge passed through the electrode, F is Faraday constant (96485 C mol^{-1}), the number 2 means two moles electrons per mole H_2, the number 1 means one mole H_2, V_m is the molar volume of gas (24.5 L mol^{-1}, 298 K, 101 KPa).

Computational details

In this work, DFT (Density Functional Theory) calculations were carried out using the CASTEP package. Generalized gradient approximation with the Perdew-Burke-Ernzerhof functional was used to describe the exchange-correlation interaction[1, 2]. The vacuum slab of 10 Å was applied in z direction to avoid the periodic interactions. The energy cut-off for the plane-wave basis set was set to 500 eV for all relaxation, energy and electronic properties calculations. The Brillouin zone was sampled with Monkhorst-Pack 2×2×1 k-points generated manually. A Gaussian smearing with a width of 0.05 eV was used in all calculations. The convergence tolerance of energy was set to 2.0×10^{-6} eV/atoms. The maximal displacement and force are 2.0×10^{-3} Å and 0.05 eV/Å, respectively. The Gibbs free energy change (ΔG) of every elemental step was calculated by using the standard hydrogen electrode (SHE) model proposed by Nørskov et al. one-half of the chemical potential of hydrogen as the chemical potential of the proton−electron pair ($H_2 \rightleftharpoons 2H^+ + 2e^-$)[3], The ΔG value can be determined as follows: $\Delta G = \Delta E + \Delta ZPE - T\Delta S + \Delta GU + \Delta G_{pH}$, where ΔE is the

adsorption energy, ΔZPE the change in zero-point energies, T the absolute temperature (T =298.15 K), ΔS the change of entropy, ΔGU the free energy contribution connected to electrode potential U. The PH value is set to 0 in this calculation. The entropies and vibrational frequencies of molecules in the gas phase are taken from the NIST database [http://cccbdb.nist.gov/].

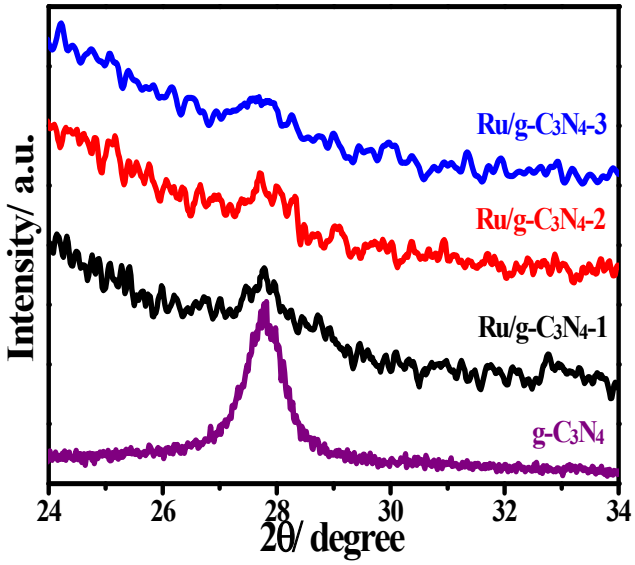

Figure S1. The corresponding partial enlargement of XRD patterns of the g-C_3N_4 and Ru/g-C_3N_4.

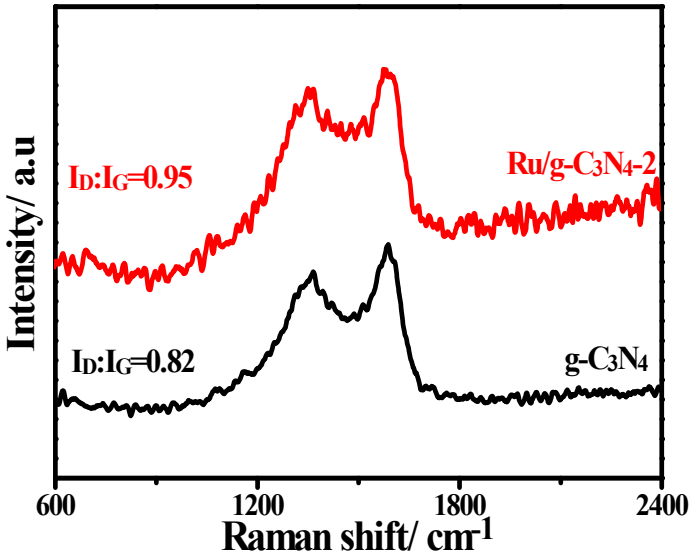

Figure S2. The Raman spectra of the g-C_3N_4 and Ru/g-C_3N_4-2.

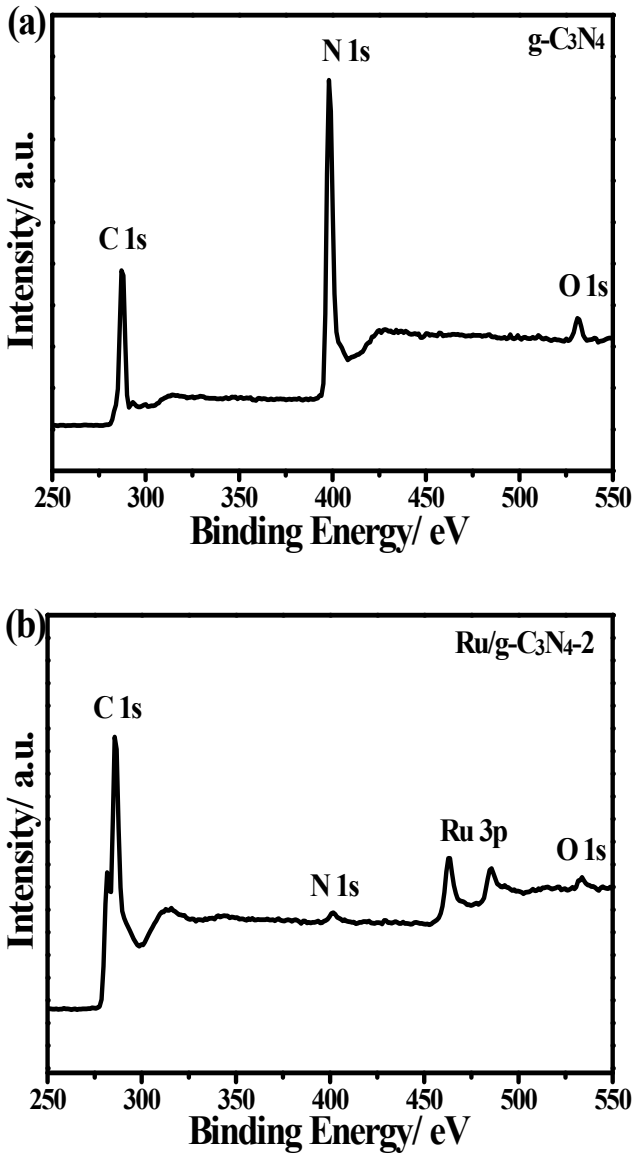

Figure S3. The whole full-scan XPS survey spectra of the g-C_3N_4 (a) and Ru/g-C_3N_4-2 (b).

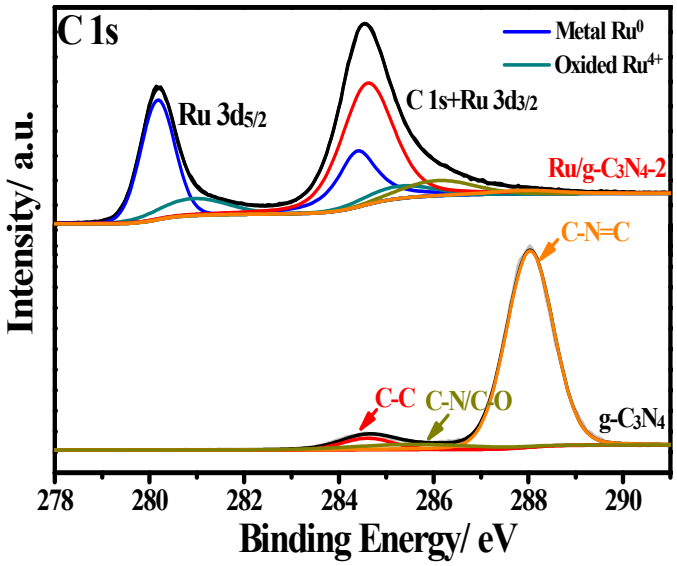

Figure S4. High-resolution XPS spectra of C 1s of the g-C_3N_4 and Ru/g-C_3N_4-2.

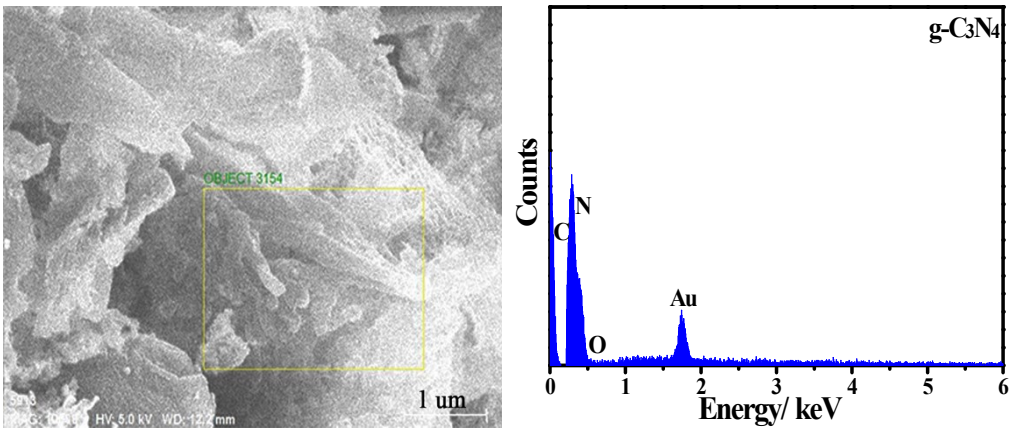

Figure S5. SEM image of the g-C_3N_4 catalyst and corresponding EDS spectrum.

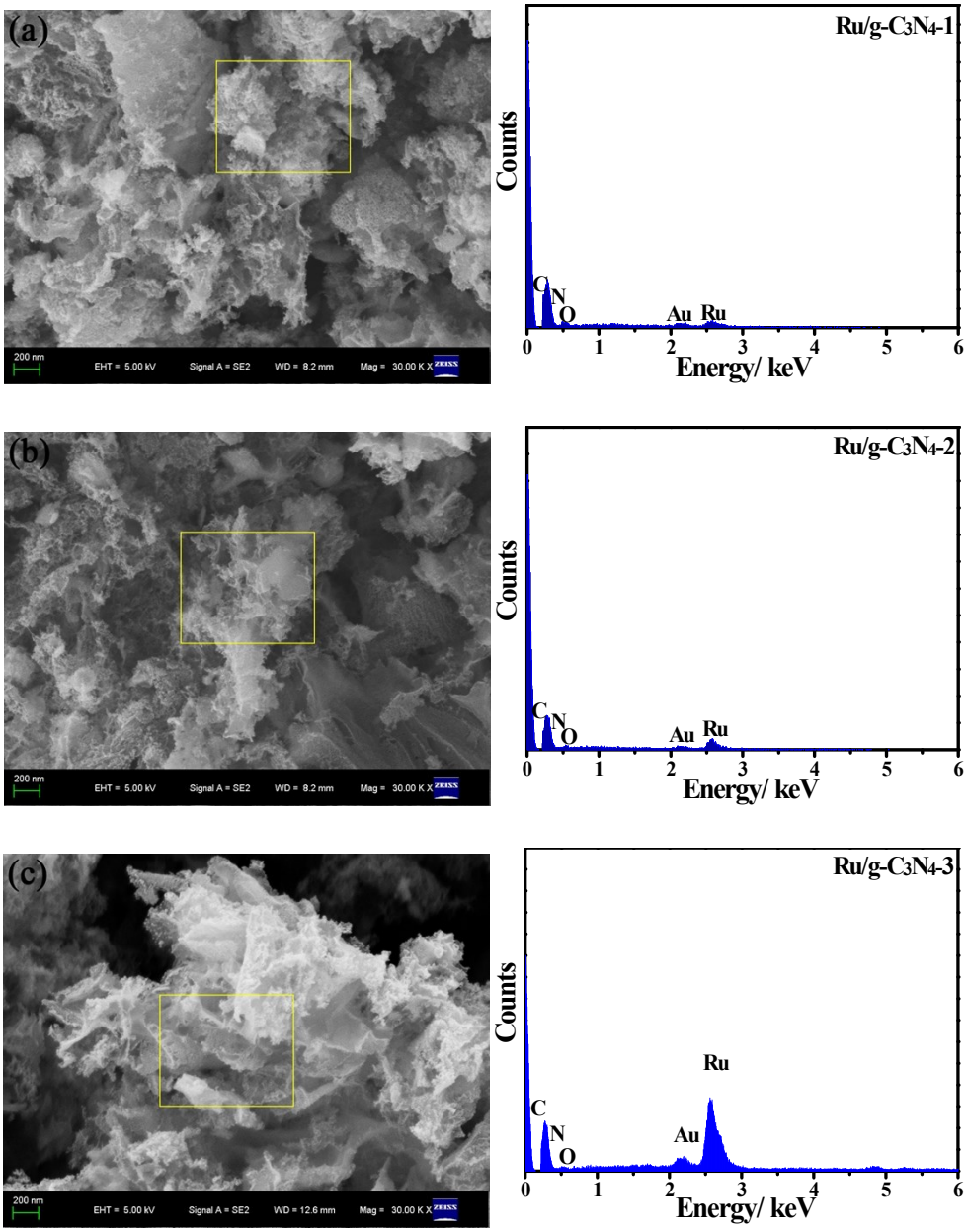

Figure S6. SEM images of (a) Ru/ g-C_3N_4-1, (b) Ru/ g-C_3N_4-2, and (c) Ru/ g-C_3N_4-3 catalysts, and corresponding EDS spectrums.

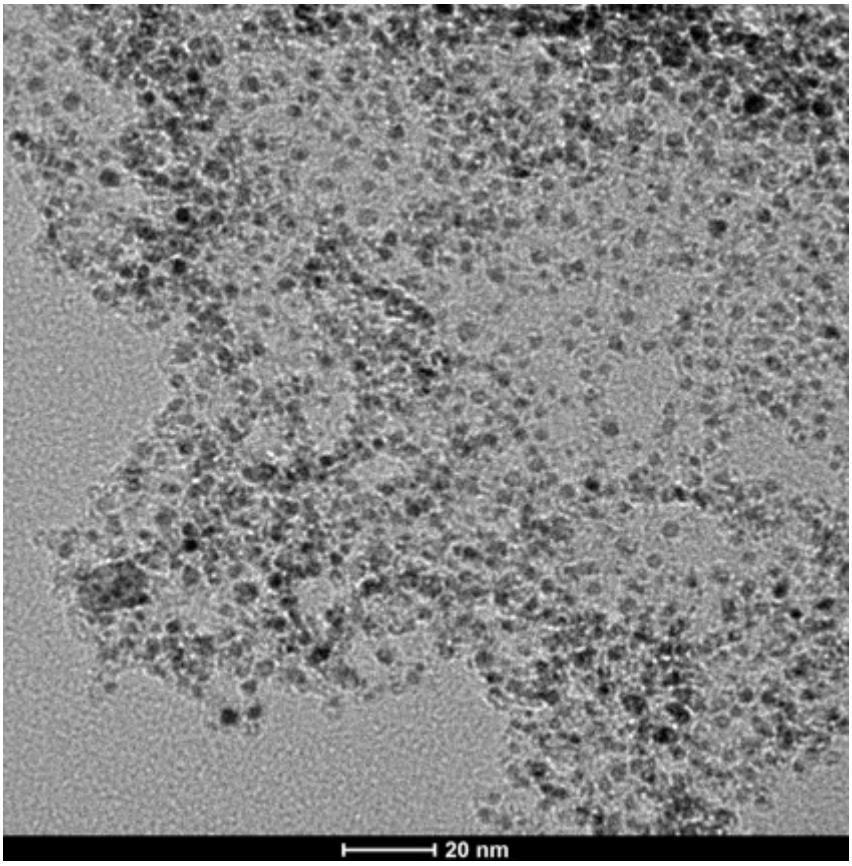

Figure S7. The TEM image of Ru/g-C_3N_4-2 catalyst.

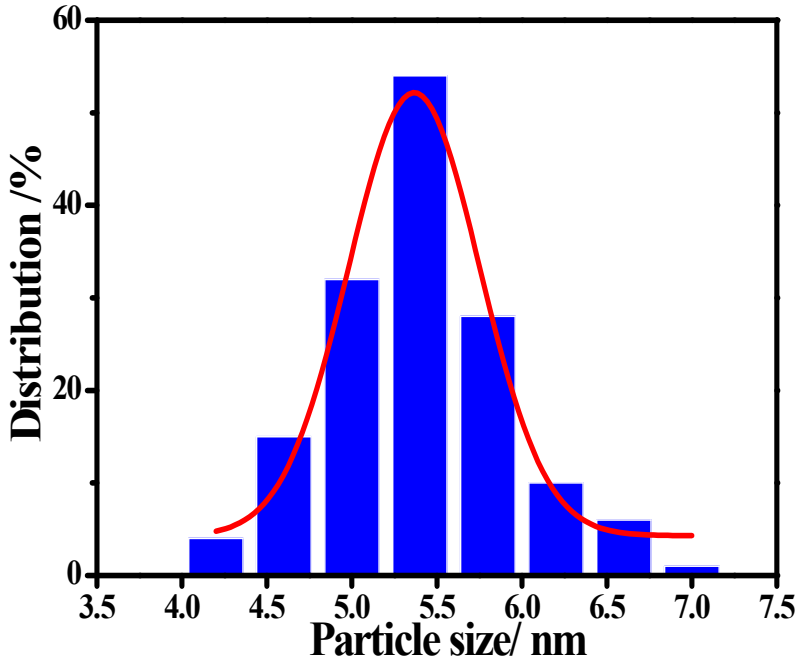

Figure S8. The size distribution histogram of Ru nanoparticles for Ru/g-C_3N_4-2 catalyst.

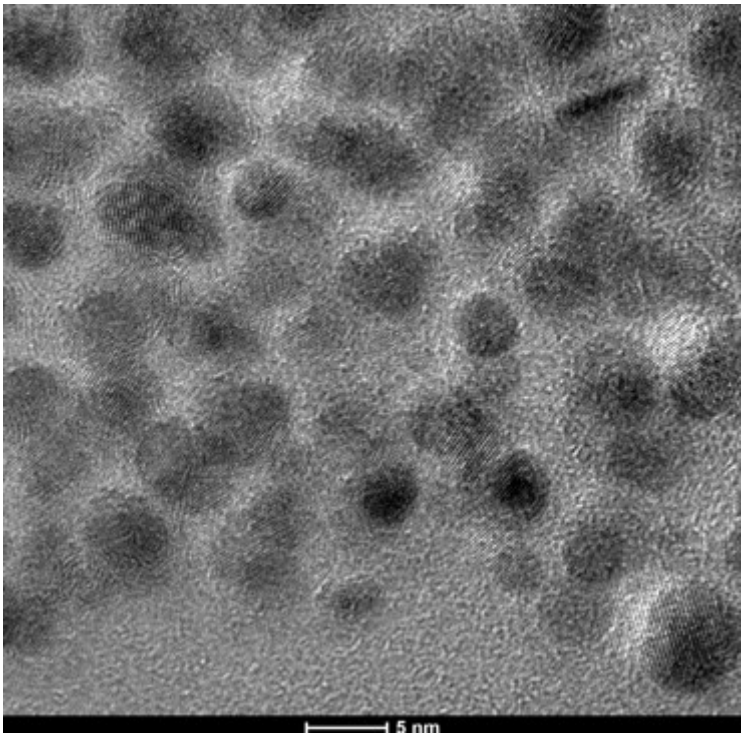

Figure S9. The high-resolution TEM image of Ru/g-C_3N_4-2 catalyst.

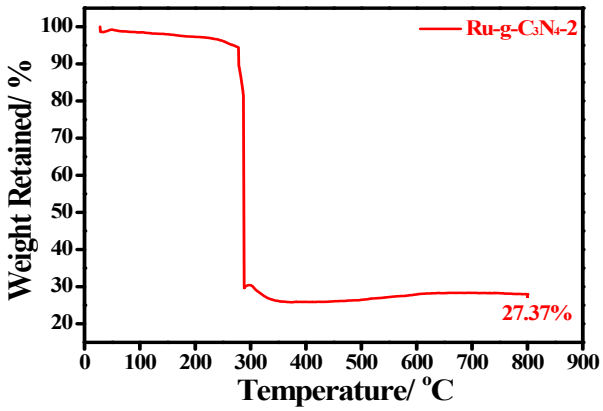

Figure S10. The thermogravimetric analysis curve of Ru-g-C_3N_4-2.

The thermogravimetric analysis was conducted in an air atmosphere in the range of 30 °C ~ 800 °C with a heating rate of 10 °C/min. The metallic Ru in Ru-g-C_3N_4-2 catalyst was considered convert to RuO_2 totally. The mass fraction of metallic Ru was ca. 20.9%.

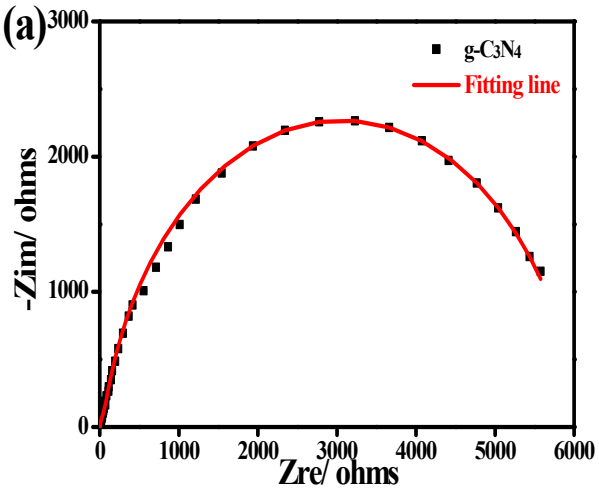

Figure S11a. Nyquist plot of the bulk g-C_3N_4 recorded in 0.5 M H_2SO_4 solution at the potential of −0.050 V vs. RHE.

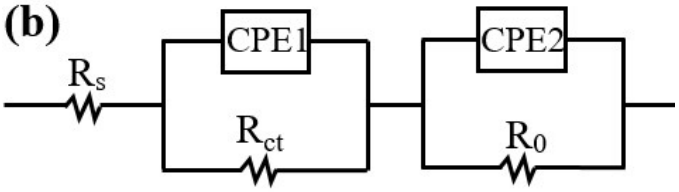

Figure S11b. Equivalent circuit diagram for Nyquist plot fitting, where R_s is the resistance of the electrolyte and the intrinsic resistance of the active materials that are modified on the electrode, R_{ct} represents the charge transfer resistance and R_0 stands for the adsorption resistance. CPE1 represents the capacitance components of an electrode porosity response and CPE2 corresponds to the HER charge-transfer double-layer capacitance components in the real-world situation.

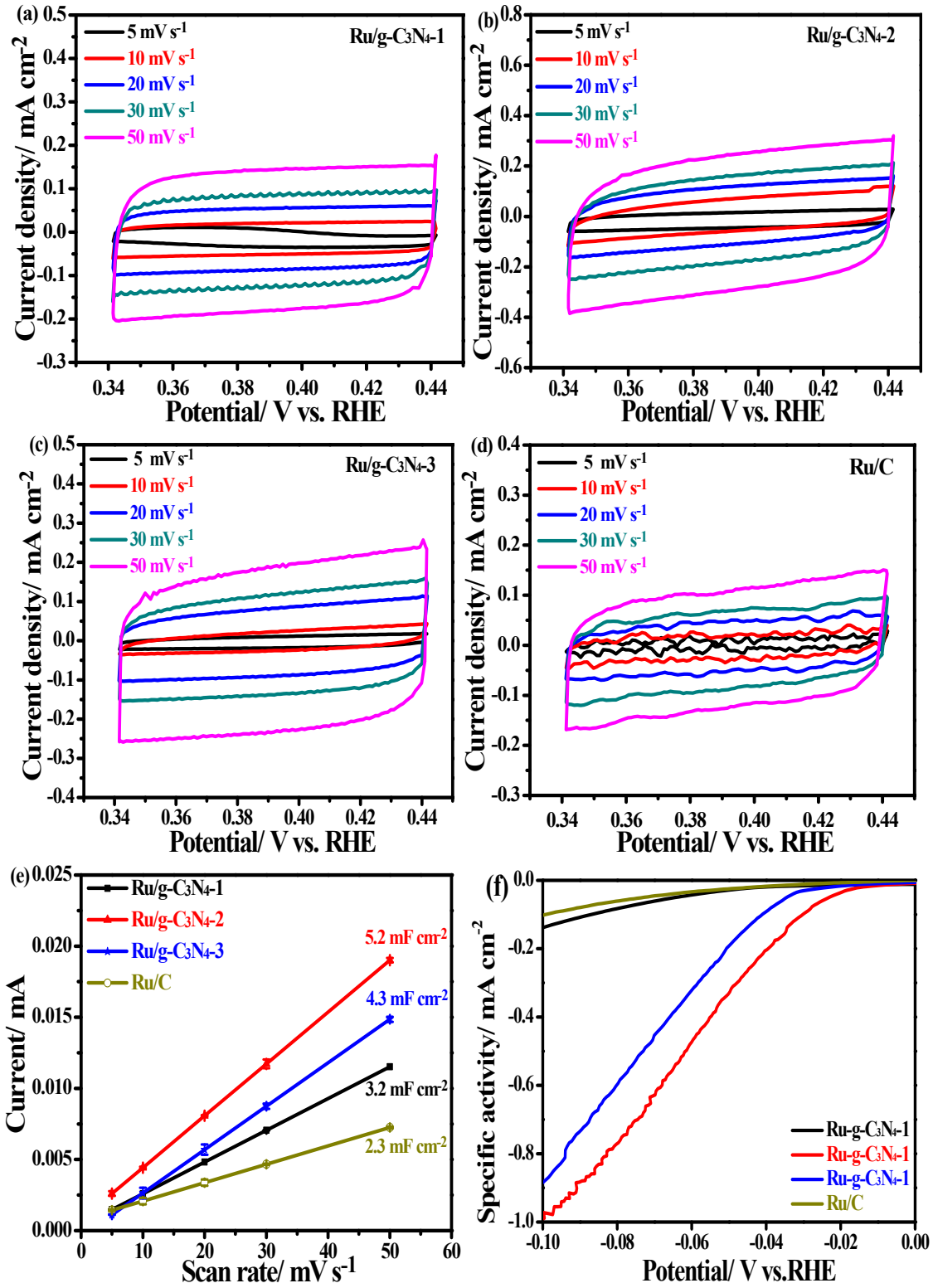

Figure S12. (a-d) Cyclic voltammograms for the double layer capacitance from 0.342 to 0.442 V, (e) the corresponding linear plots of the capacitive current versus the scan rates and (f) specific activity (normalized to the ECSA) of Ru/g-C_3N_4 and Ru/C catalysts in 0.5 M H_2SO_4 solution;

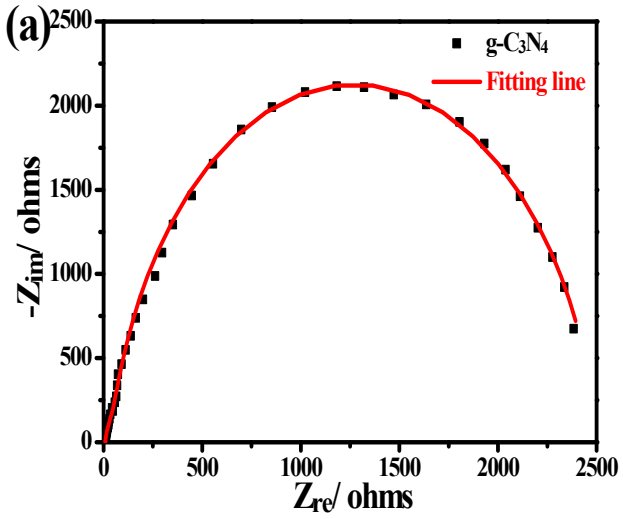

Figure S13a. Nyquist plot of the bulk g-C_3N_4 recorded in 1 M KOH solution at the potential of −0.060 V vs.RHE.

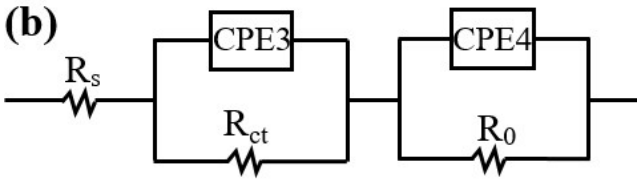

Figure S13b. Equivalent circuit diagram used to fit the Nyquist plot, where R_s is the resistance of the electrolyte and the intrinsic resistance of the active materials that are modified on the electrode, R_{ct} represents the charge transfer resistance and R_0 stands for the adsorption resistance. CPE3 represents the capacitance components of an electrode porosity response and CPE4 corresponds to the HER charge-transfer double-layer capacitance components in the real-world situation.

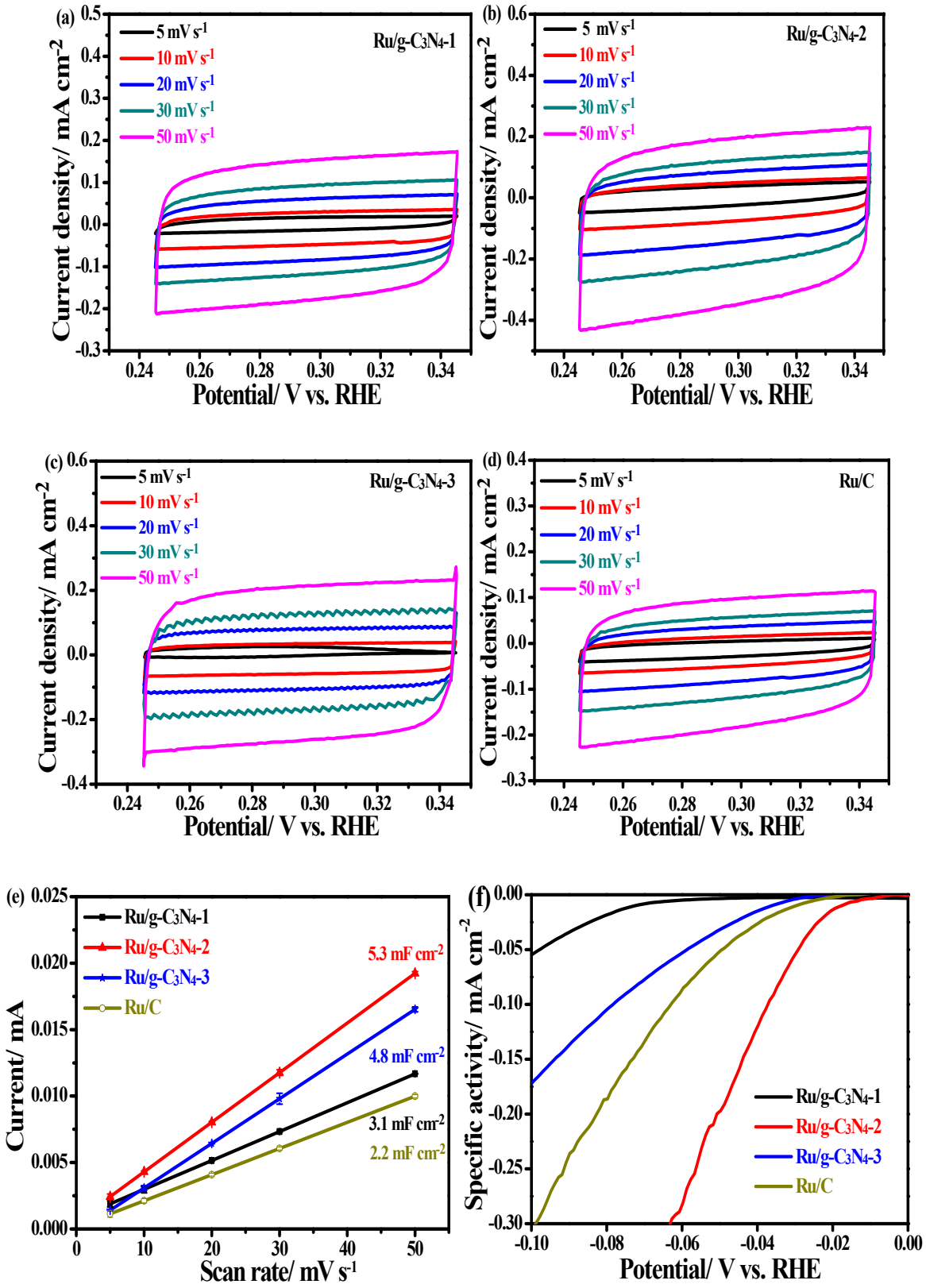

Figure S14. (a-d) Cyclic voltammograms for the double layer capacitance from 0.245 to 0.345 V; (e) the corresponding linear plots of the capacitive current versus the scan rates and (f) specific activity (normalized to the ECSA) of Ru/g-C_3N_4 and Ru/C catalysts in 1 M KOH solution;

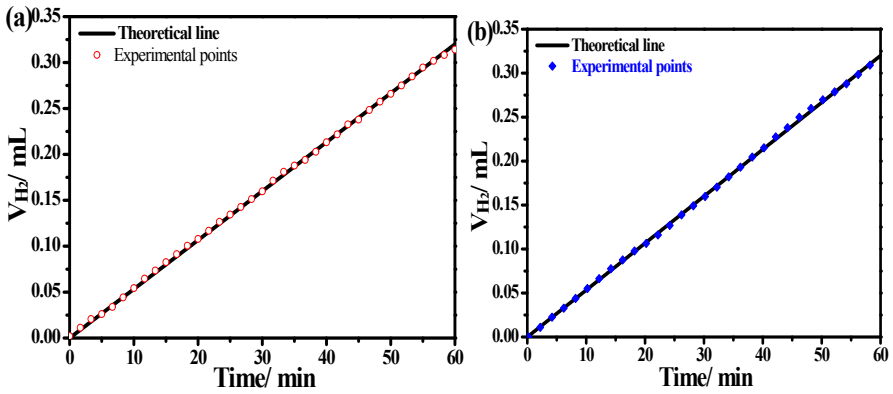

Figure S15. The amount of H_2 theoretically calculated and experimentally measured versus time for Ru/g-C_3N_4-2 in 0.5 M H_2SO_4 solution (a) and 1 M KOH solution (b) respectively. The theoretical line (black) represents the expected amounts of H_2, both assuming a nearly 100% Faradaic efficiency.

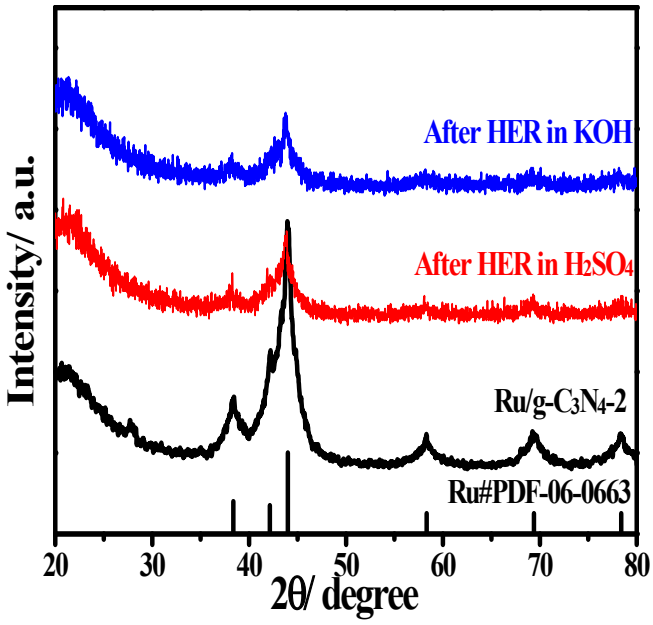

Figure S16. XRD patterns of Ru/g-C_3N_4-2 after HER electrolysis in 0.5 M H_2SO_4 solution and 1 M KOH solution.

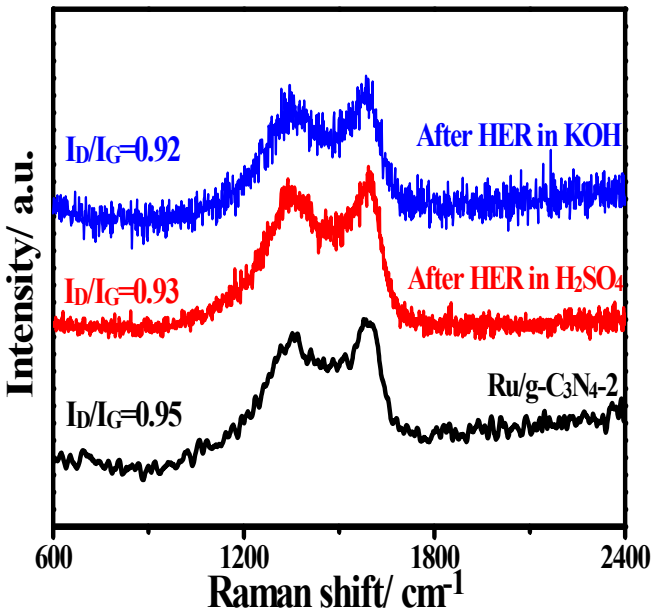

Figure S17. Raman spectra of Ru/g-C_3N_4-2 after HER electrolysis in 0.5 M H_2SO_4 solution and 1 M KOH solution.

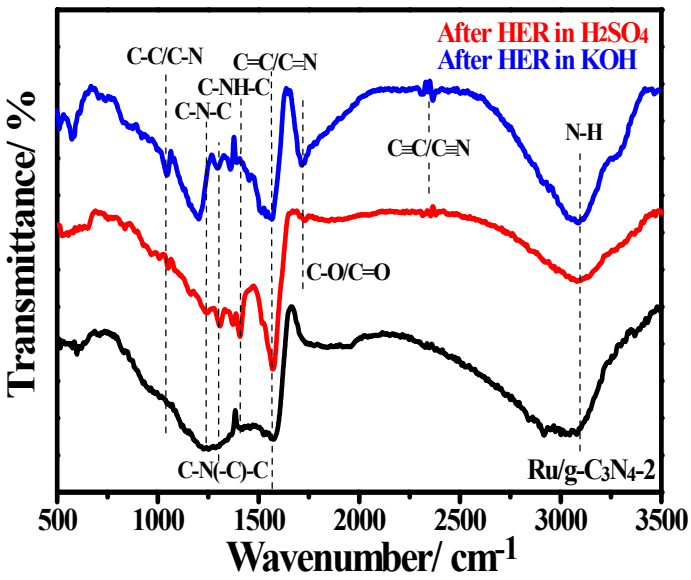

Figure S18. Fourier transforms infrared spectroscopy (FTIR) of Ru/g-C_3N_4-2 after long-term HER electrolysis in 0.5 M H_2SO_4 solution and 1 M KOH solution.

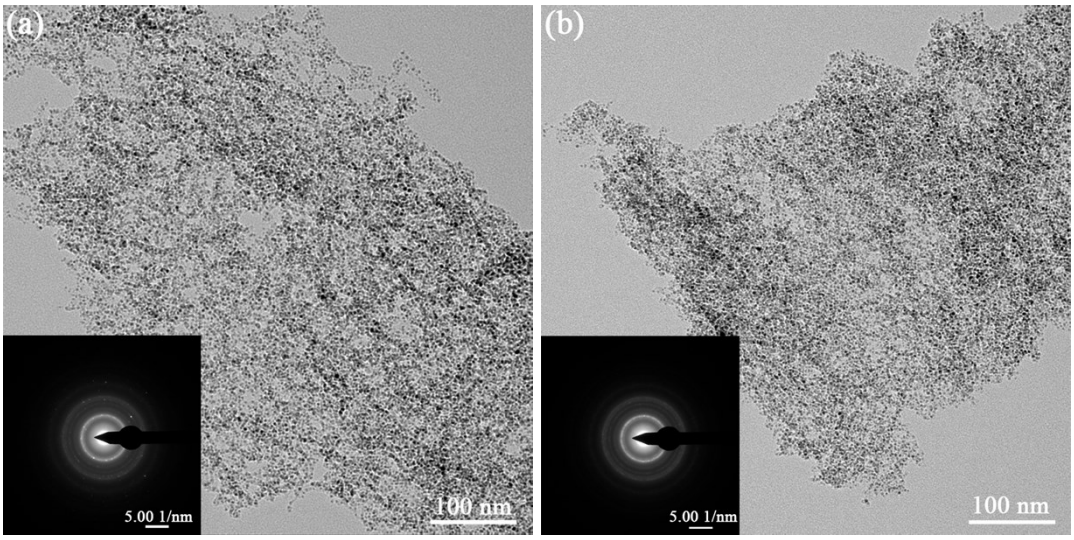

Figure S19. (a) TEM images of Ru/g-C_3N_4-2 after HER electrolysis in 0.5 M H_2SO_4 solution and (b) in 1 M KOH solution (inset: FFT images of the selected areas).

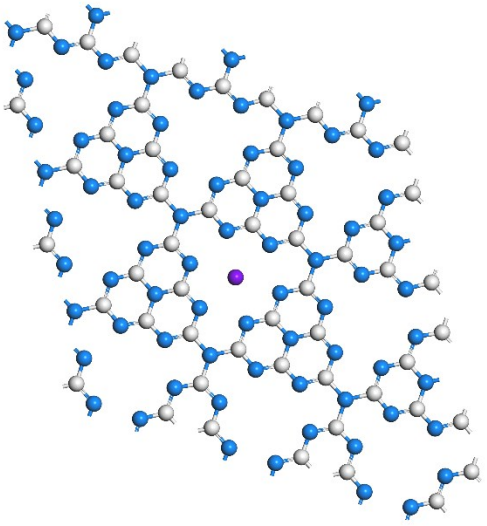

Figure S20. The optimized simplified computational models of M1.

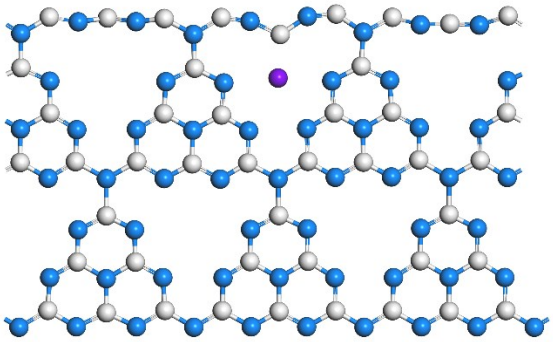

Figure S21. The optimized simplified computational models of M2.

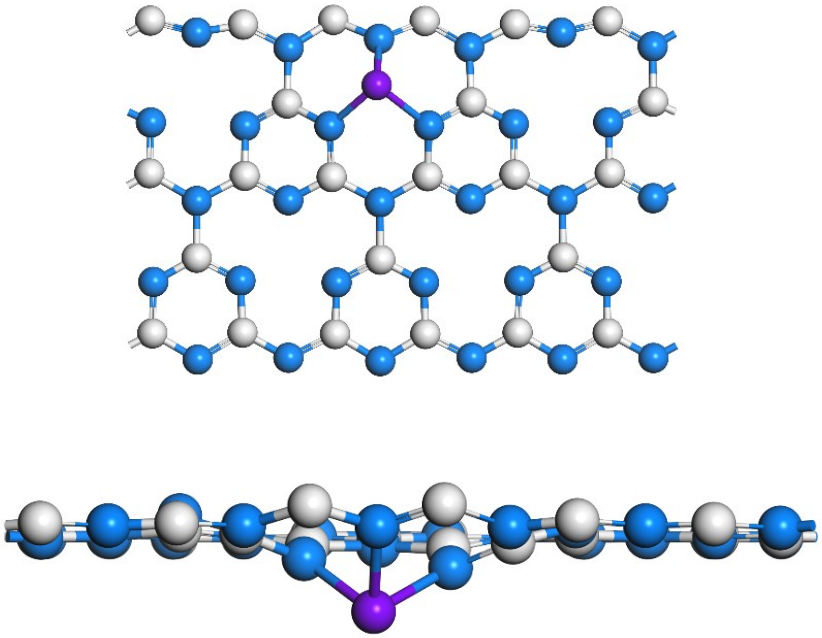

Figure S22. The optimized simplified computational models of M3 with the side view (top) and top view (bottom).

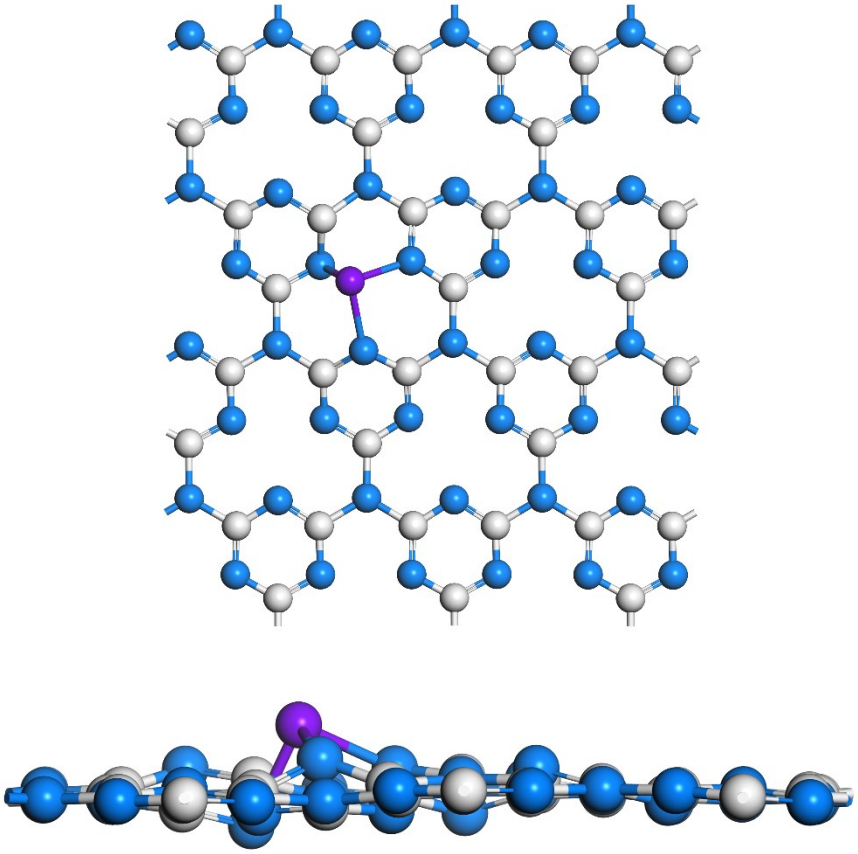

Figure S23. The optimized simplified computational models of M4 with the top view (top) and side view (bottom).

Table S1. The high-resolution XPS analysis of C 1s for g-C_3N_4 and Ru/g-C_3N_4-2 catalysts and Ru $3d_{5/2}$ for Ru/g-C_3N_4-2 catalyst.

Catalysts	C 1s			Ru $3d_{5/2}$		
	Peak	Binding energy/ eV	Relative content	Peak	Binding energy/ eV	Relative content
g-C_3N_4	C-C	284.6 eV	5%			
	C-N/C-O	285.8 eV	5%			
	C-N=C	288.0 eV	90%			
Ru/g-C_3N_4-2	C-C	284.6 eV	85%	Metal Ru^0	280.2 eV	78%
	C-N/C-O	286.1 eV	13%	Oxidized Ru^{4+}	281.0 eV	22%
	C-N=C	288.0 eV	2%			

Table S2. The high-resolution XPS analysis of N 1s for g-C_3N_4 and Ru/g-C_3N_4-2 catalysts.

Catalysts	Pyridinic-N	Pyrrolic-N	Graphitic-N	Oxidized-N
g-C_3N_4	73.2%	14.9%	8.5%	3.4%
Ru/g-C_3N_4-2	37.9%	32.7%	20.4%	9.0%

Table S3. Binding energies of the Ru 3p3/2 and Ru 3p3/2 components of Ru 3p for Ru/g-C_3N_4-2 and Ru/C catalysts

Catalysts	Ru 3p 3/2		Ru 3p 1/2	
	Peak	Binding energy/ eV	Peak	Binding energy/ eV
Ru/g-C_3N_4-2	Metal Ru	461.6	Metal Ru	483.8
	Oxidized Ru	465.5	Oxidized Ru	487.7
Ru/C	Metal Ru	462.4	Metal Ru	484.4
	Oxidized Ru	466.5	Oxidized Ru	488.5

Table S4. Element composition of the g-C_3N_4 and Ru/g-C_3N_4 catalysts obtained from quantitative EDS X-ray microanalysis results using silicon as support.

Catalysts	$C_{at.\%}$	$Ru_{at.\%}$	$N_{at.\%}$	$O_{at.\%}$	N/C ratio
g-C_3N_4	39.79	--	55.14	5.07	1.38
Ru/g- C_3N_4-1	50.82	1.24	42.68	5.26	0.84
Ru/g- C_3N_4-2	48.89	3.27	40.59	7.25	0.83
Ru/g- C_3N_4-3	47.47	4.89	38.68	8.96	0.81

Table S5. Comparison of HER performance for Pt/C and Ru/C in recent reports in acidic solution.

Materials	Electrolyte	Electrode substrate	Work Station	Overpotential(mV) @ 10 mA cm^{-2}	Reference
Pt/C	0.5 M H_2SO_4	GCE	Bio-Logic Co., France	31	This work
Pt/C	0.5 M H_2SO_4	GCE	CHI 760E	33	[4]
Pt/C	0.5 M H_2SO_4	GCE	CHI 660E	15	[5]
Pt/C	0.5 M H_2SO_4	GCE	Princeton VersaSTAT4	26	[6]
Pt/C	0.5 M H_2SO_4	GCE	CHI 760	24	[7]
Pt/C	0.5 M H_2SO_4	GCE	CHI 760E	34	[8]
Pt/C	0.5 M H_2SO_4	GCE/RDE	CHI 660D	27	[9]
Pt/C	0.5 M H_2SO_4	GCE	CHI 660E	24	[10]
Pt/C	0.5 M H_2SO_4	GCE	CHI 760D	28	[11]
Pt/C	0.5 M H_2SO_4	GCE	CHI 660E	38	[12]
Pt/C	0.5 M H_2SO_4	RDE	CHI 760D	28	[13]
Pt/C	0.5 M H_2SO_4	GCE	CHI 660E	31	[14]
Pt/C	0.5 M H_2SO_4	GCE	CHI 760E	31	[15]
Pt/C	0.5 M H_2SO_4	GC-RDE	CHI 760e	33	[16]
Pt/C	0.5 M H_2SO_4	GCE	CHI 760E	28	[17]
Pt/C	0.5 M H_2SO_4	GCE	CHI 760E	14	[18]
Pt/C	0.5 M H_2SO_4	CFP/GCDE	CHI 760E	24.1	[19]
Pt/C	0.5 M H_2SO_4	CFP	CHI 660D	47	[20]
Pt/C	0.5 M H_2SO_4	GC-RDE	CHI 760D	32	[21]
Pt/C	0.5 M H_2SO_4	GC-RDE	CHI 760 D	25	[22]
Pt/C	0.5 M H_2SO_4	GCE	CHI 760E	26	[23]
Pt/C	0.5 M H_2SO_4	GCE	CHI 760E	59	[24]
Pt/C	0.5 M H_2SO_4	GCE	Ivium	18	[25]
Pt/C	0.5 M H_2SO_4	GCE	CHI660E	39	[26]
Pt/C	0.5 M H_2SO_4	CC	CHI 760E	20	[27]
Pt/C	0.5 M H_2SO_4	GCE	CHI 760C	38	[28]
Pt/C	0.5 M H_2SO_4	GCE	CHI 630E	23	[29]

Pt/C	0.5 M H_2SO_4	GCE	Autolab PGSTAT100 potentiostat	16	[30]
Pt/C	0.5 M H_2SO_4	RDE	Ivium Technologies	13.4	[31]
Pt/C	0.5 M H_2SO_4	GCE	CHI 660C	12	[32]
Ru/C	0.5 M H_2SO_4	GCE	CHI 750E	210	[33]
Ru/C (5%)	0.5 M H_2SO_4	GCE	CHI 660E	150	[10]
Ru/C	0.5 M H_2SO_4	GCE	Bio-Logic Co., France	130	[34]
Ru/C	0.5 M H_2SO_4	GCE	CHI 760E	150	[35]

GCE: glassy carbon electrode; RDE: rotating disk electrode; RRDE: rotating ring-disk electrode; CFP: carbon fiber paper; GCRDE: glassy carbon rotating disk electrode.

Table S6. Comparison of some representative HER electrocatalysts in acidic solution.

Materials	Electrolyte	Electrode substrate	Overpotential(mV) @ 10 mA cm^{-2}	Reference
Ru/g-C_3N_4-2	0.5 M H_2SO_4	GCE	27	This work
Pt/C	0.5 M H_2SO_4	GCE	31	This work
Ru/C	0.5 M H_2SO_4	GCE	123	This work
Commercial Pt/C	0.5 M H_2SO_4	GCE	33	[4]
ALD100Pt/NGNs	0.5 M H_2SO_4	GCE	40	[36]
RuP_2@NPC	0.5 M H_2SO_4	GCE	38	[37]
Ru-MoS_2	0.5 M H_2SO_4	GCE	300	[6]
Pt-MoS_2	0.5 M H_2SO_4	GCE	139	[6]
Ru/C_3N_4/C	0.5 M H_2SO_4	GCE	60	[38]
Ni@Ni_2P-Ru	0.5 M H_2SO_4	GCE	51	[39]
Ru_2P nanoparticles	0.5 M H_2SO_4	GCE	55	[40]
Ru/GLC	0.5 M H_2SO_4	GCE	35	[41]
Ru@NG	0.5 M H_2SO_4	GCE	42	[42]
Pt-SnS_2	0.5 M H_2SO_4	GCE	117	[43]
Ru-Ru_2P/PC-2	0.5 M H_2SO_4	GCE	43	[44]
Ru/MeOH/THF	0.5 M H_2SO_4	GCE	83	[45]
Te@Ru-0.6/C	0.5 M H_2SO_4	GCE	86	[34]
Pt NCs@CIAC-121	0.5 M H_2SO_4	GCE	48	[47]
Ru@RFCS-6h	0.5 M H_2SO_4	GCE	58	[48]
$Cu_{2-x}S$@Ru NPs	0.5 M H_2SO_4	GCE	129	[49]
Ru-MoO_2	0.5 M H_2SO_4	GCE	55	[50]
$Pt_{13}Cu_{73}Ni_4$/CNF@CF	1 M H_2SO_4	GCE	70 (at 5 mA cm^{-2})	[51]
1D-RuO_2-CN_x	0.5 M H_2SO_4	GCE	93	[52]
Ru/OMSNNC	0.5 M H_2SO_4	GCE	27	[10]
Ru@MWCNT	0.5 M H_2SO_4	RRDE	13	[53]

RuNi/CQDs	0.5 M H_2SO_4	GCE	58	[54]
Ru-RuO_2/CNT	0.5 M H_2SO_4	GCE	63	[55]
Ru-HPC	0.5 M H_2SO_4	GCE	61.6	[56]
Ru-NGC	0.5 M H_2SO_4	GCE	25	[57]
Ru_2P nanoparticles	0.5 M H_2SO_4	GCE	55	[40]
RuSi	0.5 M H_2SO_4	GCE	19	[58]
RuCu NSs	0.5 M H_2SO_4	GCE	19	[59]
Ni@Ru/CNS-10%	0.5 M H_2SO_4	GCE	65	[60]
Ru-Ru_2P/PC-2ee	0.5 M H_2SO_4	GCE	43	[44]
Ru^0 /CeO_2	0.5 M H_2SO_4	GCE	47	[61]
Te@Ru-0.6/C	0.5 M H_2SO_4	GCE	86	[34]
0.27-RuO_2@C	0.5 M H_2SO_4	RRDE	33	[62]
Ru@GnP	0.5 M H_2SO_4	RRDE	13	[63]
Ru@RFCS-6h	0.5 M H_2SO_4	GCE	58	[14]
$RuIrO_x$	0.5 M H_2SO_4	CFP	12	[64]
Ru-MoO_2	0.5 M H_2SO_4	GCE	55	[50]
Ru_2P/RGO-20	0.5 M H_2SO_4	GCE	22	[65]
Ru@C_2N	0.5 M H_2SO_4	RDE	22	[46]

GCE: glassy carbon electrode; RDE: rotating disk electrode; RRDE: rotating ring-disk electrode; CFP: carbon fiber paper; GCRDE: glassy carbon rotating disk electrode.

Table S7. EIS fitting parameters from equivalent circuits for different catalysts in 0.5 M H_2SO_4 solution.

Catalysts	R_s/ Ω	R_{ct}/ Ω	CPE/ S s^{-n}	R_0/ Ω	CPE/ S s^{-n}
Ru/g-C_3N_4-1	9.0	95.3	2.2E-3	82.2	3.3E-4
Ru/g-C_3N_4-2	8.8	32.2	3.8E-4	50.3	4.3E-5
Ru/g-C_3N_4-3	8.7	45.4	4.6E-4	64.6	5.6E-5
Ru/C	9.0	113.7	2.4 E-3	91.8	3.5E-4

Table S8. Mass activity and TOFs at the overpotential of 0.05 V vs. RHE of different catalysts in 0.5 M H_2SO_4 solution.

Catalysts	Mass activity/ mA mg^{-1}	TOF/ s^{-1}
Ru/g-C_3N_4-1	-31.0	0.05
Ru/g-C_3N_4-2	-554.3	0.85
Ru/g-C_3N_4-3	-203.6	0.32
Ru/C	-20.3	0.03

Table S9. Double-layer capacitance (C_{dl}), electrochemical surface areas (ECSA) and roughness factor of different catalysts in 0.5 M H_2SO_4 solution.

Catalysts	C_{dl}/ mF	ECSA/ cm^2	Roughness Factor
Ru/g-C_3N_4-1	0.22	5.50	78.57
Ru/g-C_3N_4-2	0.36	9.00	128.57
Ru/g-C_3N_4-3	0.30	7.50	107.14
Ru/C	0.16	4.03	57.57

Table S10. Comparison of HER performance for Pt/C and Ru/C in recent reports in alkaline solution.

Materials	Electrolyte	Electrode substrate	Work Station	Overpotential(mV) @ 10 mA cm^{-2}	Reference
Pt/C	1 M KOH	GCE	Bio-Logic Co., France	49	This work
Pt/C	1 M KOH	GCE	CHI 760	58	[7]
Pt/C	1 M KOH	GCE	CHI 660E	45	[66]
Pt/C	1 M KOH	RDE	CHI 660D	38	[9]
Pt/C	1 M KOH	GCE	CHI 660E	32	[10]
Pt/C	1 M KOH	GCE	CHI 760D	49	[11]
Pt/C	1 M KOH	GCE	CHI 750E	39	[67]
Pt/C	1 M KOH	GCE	CHI 660E	38	[12]
Pt/C	1 M KOH	GCE	CHI 760	32.7	[68]
Pt/C	1 M KOH	GCE	CHI 760E	48	[69]
Pt/C	1 M KOH	CFP/GCDE	CHI 760E	53.7	[19]
Pt/C	1 M KOH	CFP	CHI 660D	52	[20]
Pt/C	1 M KOH	GC-RDE	CHI 760D	30	[21]
Pt/C	1 M KOH	GC-RDE	CHI 760 D	53	[22]
Pt/C	1 M KOH	GC-RDE	CHI760	91	[70]
Pt/C	1 M KOH	GCE	CHI 600E	46	[71]
Pt/C	1 M KOH	RDE	CHI 660D	55.6	[72]
Pt/C	1 M KOH	GCE	Gamry (Interface 1000E, USA)	53.4	[44]
Pt/C	1 M KOH	carbon cloth	Biologic VMP3	49	[73]
Pt/C	1 M KOH	CC	CHI 760E	25	[27]
Pt/C	1 M KOH	GCE	CHI 760	30	[74]
Pt/C	1 M KOH	CFP	CHI 760E	44.7	[75]
Pt/C	1 M KOH	GCE	CHI 630E	26	[29]
Pt/C	1 M KOH	GCE	CHI 760E	44	[76]
Pt/C	1 M KOH	GCE	CHI 660D	38	[77]
Pt/C	1 M KOH	GCE	CHI 660C	92	[32]
Ru/C	1 M KOH	GCE	CHI 750E	186	[33]

Ru/C	1 M KOH	GCE	Ivium CompactStat. h	100	[78]
Ru/C	1 M KOH	GCE	Gamry (Interface 1000E, USA)	57	[44]
Ru/C (5%)	1 M KOH	GCE	CHI 760E	94	[79]
Ru/C (5%)	1 M KOH	GCE	CHI 660E	62	[10]
Ru/C	1 M KOH	GCE	Autolab electrochemical workstation (PGSTAT12)	70	[80]
Ru/C	1 M KOH	GCE	CHI 760E	139	[35]
Ru/C	1 M KOH	GCE	(Bio-Logic Co., France)	80	[81]

GCE: glassy carbon electrode; RDE: rotating disk electrode; RRDE: rotating ring-disk electrode; CFP: carbon fiber paper; GCRDE: glassy carbon rotating disk electrode.

Table S11. Comparison of some representative HER electrocatalysts in alkaline solution.

Materials	Electrolyte	Electrode substrate	Overpotential/ mV @ 10 mA cm^{-2}	Reference
Ru/g-C_3N_4-2	1 M KOH	GCE	34	This work
Pt/C	1 M KOH	GCE	49	This work
Ru/C	1 M KOH	GCE	82	This work
RuP_2@NPC	1 M KOH	GCE	52	[37]
RuP_2 nanoparticles	1 M KOH	GCE	90	[37]
Ru/C_3N_4/C	1 M KOH	GCE	79	[38]
Ru_2P	1 M KOH	GCE	50	[40]
Pt@C_2N	1 M KOH	GCRDE	100	[46]
Ru@C_2N	1 M KOH	RDE	17	[46]
$Cu_{2-x}S$@Ru NPs	1 M KOH	GCE	82	[49]
1D-RuO_2-CN_x	0.5 M KOH	GCE	95	[52]
Commercial Pt/C	1 M KOH	GCE	80	[82]
RuP_x@NPC	1 M KOH	GCE	74	[83]
Pt NWs/SL-$Ni(OH)_2$	1 M KOH	GCE	57 (at 4 mA cm^{-2})	[84]
hcp-Ru@NC-700	1 M KOH	GCE	120	[85]
Pt-$Co(OH)_2$/CC	1 M KOH	GCE	70	[86]
Ru/CP	1 M KOH	Carbon paper	78	[87]
Pt-NiFe LDH	1 M KOH	GCE	106	[88]
Ru/C	1 M KOH	Carbon paper	56	[89]
Ru/OMSNNC	1 M KOH	GCE	13	[10]
Ru@MWCNT	1 M KOH	RRDE	17	[53]
Ru NCs/BNG	1 M KOH	GCE	14	[90]
RuNi/CQDs	1 M KOH	GCE	13	[54]
Ru-HPC	1 M KOH	GCE	4	[56]
Ru-NC-700	1 M KOH	GCE	12	[91]

Ru-RuO_2/CNT	1 M KOH	GCE	12	[55]
Ru/3DNPC-500	1 M KOH	GCE	15	[92]
Commercial Pt/C	1 M KOH	GCE	32	[10]
Ru-NGC	1 M KOH	GCE	37	[57]
Ru@NC	1 M KOH	Carbon paper	26	[93]
Ru@CN	1 M KOH	GCE	32	[94]
Ru@GnP	1 M KOH	RRDE	22	[63]
Ru@NCHNSs	1 M KOH	GCE	28	[95]

GCE: glassy carbon electrode; RDE: rotating disk electrode; RRDE: rotating ring-disk electrode; GCRDE: glassy carbon rotating disk electrode.

Table S12. EIS fitting parameters from equivalent circuits for different catalysts in 1 M KOH solution.

Catalysts	R_s/ Ω	R_{ct}/ Ω	CPE/ S s^{-n}	R_0/ Ω	CPE/ S s^{-n}
Ru/g-C_3N_4-1	8.9	99.6	6.5E-4	65.2	4.7E-4
Ru/g-C_3N_4-2	8.5	35.2	4.2E-4	33.4	3.1E-5
Ru/g-C_3N_4-3	8.6	55.1	5.3E-4	44.7	4.2E-5
Ru/C	8.6	65.3	5.8E-3	59.3	4.5E-4

Table S13. Double-layer capacitance (C_{dl}), electrochemical surface areas (ECSA) and roughness factor of different catalysts in 1 M KOH solution.

Catalysts	C_{dl}/ mF	ECSA/ cm^2	Roughness Factor
Ru/g-C_3N_4-1	0.22	5.50	78.57
Ru/g-C_3N_4-2	0.37	9.25	132.14
Ru/g-C_3N_4-3	0.34	8.50	121.43
Ru/C	0.15	3.75	53.57

Table S14. Mass activity and TOFs at the overpotential of 0.05 V vs. RHE of different catalysts in 1 M KOH solution.

Catalysts	Mass activity/ mA mg^{-1}	TOF/ s^{-1}
Ru/g-C_3N_4-1	-7.9	0.01
Ru/g-C_3N_4-2	-322.1	0.51
Ru/g-C_3N_4-3	-48.0	0.06
Ru/C	-29.0	0.04

References

1. J. P. Perdew, K. Burke and M. Ernzerhof, *Phys. Rev. Lett.*, 1996, **77**, 3865-3868.
2. B. Hinnemann, P. G. Moses, J. Bonde, K. P. Jørgensen, J. H. Nielsen, S. Horch, I. Chorkendorff and J. K. Nørskov, *J. Am. Chem. Soc.*, 2005, **127**, 5308-5309.
3. E. Skúlason, T. Bligaard, S. Gudmundsdóttir, F. Studt, J. Rossmeisl, F. Abild-Pedersen, T. Vegge, H. Jónsson and J. K. Nørskov, *Phys. Chem. Chem. Phys.*, 2012, **14**, 1235-1245.
4. F.-Y. Yu, Z.-L. Lang, L.-Y. Yin, K. Feng, Y.-J. Xia, H.-Q. Tan, H.-T. Zhu, J. Zhong, Z.-H. Kang and Y.-G. Li, *Nat. Commun.*, 2020, **11**, 490.
5. S. Ye, F. Luo, Q. Zhang, P. Zhang, T. Xu, Q. Wang, D. He, L. Guo, Y. Zhang, C. He, X. Ouyang, M. Gu, J. Liu and X. Sun, *Energy & Environmental Science*, 2019, **12**, 1000-1007.
6. Y. Cheng, S. Lu, F. Liao, L. Liu, Y. Li and M. Shao, *Advanced Functional Materials*, 2017, **27**, 1700359.
7. F. Yang, Y. Zhao, Y. Du, Y. Chen, G. Cheng, S. Chen and W. Luo, *Adv. Energy Mater.*, 2018, **8**, 1703489.
8. H. Tian, X. Cui, L. Zeng, L. Su, Y. Song and J. Shi, *J. Mater. Chem. A*, 2019, **7**, 6285-6293.
9. Z. Han, R.-L. Zhang, J.-J. Duan, A.-J. Wang, Q.-L. Zhang, H. Huang and J.-J. Feng, *International Journal of Hydrogen Energy*, 2020, **45**, 6110-6119.
10. Y.-L. Wu, X. Li, Y.-S. Wei, Z. Fu, W. Wei, X.-T. Wu, Q.-L. Zhu and Q. Xu, *Advanced Materials*, 2021, **33**, 2006965.
11. F. Zhang, Y. Zhu, Y. Chen, Y. Lu, Q. Lin, L. Zhang, S. Tao, X. Zhang and H. Wang, *J. Mater. Chem. A*, 2020, **8**, 12810-12820.
12. C. Zhang, P. Wang, W. Li, Z. Zhang, J. Zhu, Z. Pu, Y. Zhao and S. Mu, *J. Mater. Chem. A*, 2020, **8**, 19348-19356.

13. C. Li, Z. Chen, H. Yi, Y. Cao, L. Du, Y. Hu, F. Kong, R. Kramer Campen, Y. Gao, C. Du, G. Yin, I. Y. Zhang and Y. Tong, *Angew. Chem. Int. Ed.*, 2020, **59**, 15902-15907.
14. W. Chen, J. Pei, C.-T. He, J. Wan, H. Ren, Y. Wang, J. Dong, K. Wu, W.-C. Cheong, J. Mao, X. Zheng, W. Yan, Z. Zhuang, C. Chen, Q. Peng, D. Wang and Y. Li, *Adv. Mater.*, 2018, **30**, 1800396.
15. F. Lu, D. Yi, S. Liu, F. Zhan, B. Zhou, L. Gu, D. Golberg, X. Wang and J. Yao, *Angew. Chem. Int. Ed.*, 2020, **59**, 17712-17718.
16. T. Liu, W. Gao, Q. Wang, M. Dou, Z. Zhang and F. Wang, *Angew. Chem. Int. Ed.*, 2020, **59**, 20423-20427.
17. C. Xie, W. Chen, S. Du, D. Yan, Y. Zhang, J. Chen, B. Liu and S. Wang, *Nano Energy*, 2020, **71**, 104653.
18. H. Jin, S. Sultan, M. Ha, J. N. Tiwari, M. G. Kim and K. S. Kim, *Adv. Funct. Mater.*, 2020, **30**, 2000531.
19. X.-K. Wan, H. B. Wu, B. Y. Guan, D. Luan and X. W. Lou, *Adv. Mater.*, 2020, **32**, 1901349.
20. H. Zhang, W. Zhou, X. F. Lu, T. Chen and X. W. Lou, *Adv. Energy Mater.*, 2020, **10**, 2000882.
21. E. Cao, Z. Chen, H. Wu, P. Yu, Y. Wang, F. Xiao, S. Chen, S. Du, Y. Xie, Y. Wu and Z. Ren, *Angew. Chem. Int. Ed.*, 2020, **59**, 4154-4160.
22. L. Xiu, W. Pei, S. Zhou, Z. Wang, P. Yang, J. Zhao and J. Qiu, *Adv. Funct. Mater.*, 2020, **30**, 1910028.
23. M. Song, Y. Song, H. Li, P. Liu, B. Xu, H. Wei, J. Guo and Y. Wu, *Electrochimica Acta*, 2019, **320**, 134603.
24. L. Zhang, Y. Jia, H. Liu, L. Zhuang, X. Yan, C. Lang, X. Wang, D. Yang, K. Huang, S. Feng and X. Yao, *Angew. Chem. Int. Ed.*, 2019, **58**, 9404-9408.
25. F. Li, G.-F. Han, H.-J. Noh, J.-P. Jeon, I. Ahmad, S. Chen, C. Yang, Y. Bu, Z. Fu, Y. Lu and J.-B. Baek, *Nat. Commun.*, 2019, **10**, 4060.
26. J. Li, C. Cao and H. Zhu, *Nanotechnology*, 2007, **18**, 115605.
27. T. Liu, P. Li, N. Yao, G. Cheng, S. Chen, W. Luo and Y. Yin, *Angew. Chem. Int. Ed.*, 2019, **58**, 4679-4684.
28. X. Li, J. Yu, J. Jia, A. Wang, L. Zhao, T. Xiong, H. Liu and W. Zhou, *Nano Energy*, 2019, **62**, 127-135.
29. B. Yang, J. Xu, D. Bin, J. Wang, J. Zhao, Y. Liu, B. Li, X. Fang, Y. Liu, L. Qiao, L. Liu and B. Liu, *Appl. Catal. B: Environ.*, 2021, **283**, 119583.
30. T. Rajala, R. Kronberg, R. Backhouse, M. E. M. Buan, M. Tripathi, A. Zitolo, H. Jiang, K. Laasonen, T. Susi, F. Jaouen and T. Kallio, *Appl. Catal. B: Environ.*, 2020, **265**, 118582.
31. M. Kim, M. A. R. Anjum, M. Lee, B. J. Lee and J. S. Lee, *Adv. Funct. Mater.*, 2019, **29**, 1809151.
32. S.-W. Sun, G.-F. Wang, Y. Zhou, F.-B. Wang and X.-H. Xia, *ACS Appl. Mater. Interfaces*, 2019, **11**, 19176-19182.
33. Z. Ding, K. Wang, Z. Mai, G. He, Z. Liu and Z. Tang, *International Journal of Hydrogen Energy*, 2019, **44**, 24680-24689.
34. X. Yang, Z. Zhao, X. Yu and L. Feng, *Chem. Commun.*, 2019, **55**, 1490-1493.
35. J. Yu, Y. Guo, S. She, S. Miao, M. Ni, W. Zhou, M. Liu and Z. Shao, *Adv. Mater.*, 2018, **30**, 1800047.
36. N. Cheng, S. Stambula, D. Wang, M. N. Banis, J. Liu, A. Riese, B. Xiao, R. Li, T.-K. Sham, L.-M. Liu, G. A. Botton and X. Sun, *Nat. Commun.*, 2016, **7**, 13638.
37. Z. Pu, I. S. Amiinu, Z. Kou, W. Li and S. Mu, *Angew. Chem. Int. Ed.*, 2017, **56**, 11559-11564.

38. Y. Zheng, Y. Jiao, Y. Zhu, L. H. Li, Y. Han, Y. Chen, M. Jaroniec and S.-Z. Qiao, *J. Am. Chem. Soc.*, 2016, **138**, 16174-16181.
39. Y. Liu, S. Liu, Y. Wang, Q. Zhang, L. Gu, S. Zhao, D. Xu, Y. Li, J. Bao and Z. Dai, *J. Am. Chem. Soc.*, 2018, **140**, 2731-2734.
40. Y. Wang, Z. Liu, H. Liu, N.-T. Suen, X. Yu and L. Feng, *ChemSusChem*, 2018, **11**, 2724-2729.
41. Z. Chen, J. Lu, Y. Ai, Y. Ji, T. Adschiri and L. Wan, *ACS Appl. Mater. Interfaces*, 2016, **8**, 35132-35137.
42. J. Yang, H. Guo, S. Chen, Y. Li, C. Cai, P. Gao, L. Wang, Y. Zhang, R. Sun, X. Niu and Z. Wang, *J. Mater. Chem. A*, 2018, **6**, 13859-13866.
43. B. Wang, L. Xu, G. Liu, P. Zhang, W. Zhu, J. Xia and H. Li, *J. Mater. Chem. A*, 2017, **5**, 20170-20179.
44. Z. Liu, Z. Li, J. Li, J. Xiong, S. Zhou, J. Liang, W. Cai, C. Wang, Z. Yang and H. Cheng, *Journal of Materials Chemistry A*, 2019, **7**, 5621-5625.
45. S. Drouet, J. Creus, V. Collière, C. Amiens, J. García-Antón, X. Sala and K. Philippot, *Chem. Commun.*, 2017, **53**, 11713-11716.
46. J. Mahmood, F. Li, S.-M. Jung, M. S. Okyay, I. Ahmad, S.-J. Kim, N. Park, H. Y. Jeong and J.-B. Baek, *Nature Nanotechnology*, 2017, **12**, 441-446.
47. S. Wang, X. Gao, X. Hang, X. Zhu, H. Han, W. Liao and W. Chen, *J. Am. Chem. Soc.*, 2016, **138**, 16236-16239.
48. K. Li, Y. Li, Y. Wang, J. Ge, C. Liu and W. Xing, *Energy Environ. Sci.*, 2018, **11**, 1232-1239.
49. D. Yoon, J. Lee, B. Seo, B. Kim, H. Baik, S. H. Joo and K. Lee, *Small*, 2017, **13**, 1700052.
50. P. Jiang, Y. Yang, R. Shi, G. Xia, J. Chen, J. Su and Q. Chen, *J. Mater. Chem. A*, 2017, **5**, 5475-5485.
51. Y. Shen, A. C. Lua, J. Xi and X. Qiu, *ACS Appl. Mater. Interfaces*, 2016, **8**, 3464-3472.
52. T. Bhowmik, M. K. Kundu and S. Barman, *ACS Appl. Mater. Interfaces*, 2016, **8**, 28678-28688.
53. D. H. Kweon, M. S. Okyay, S.-J. Kim, J.-P. Jeon, H.-J. Noh, N. Park, J. Mahmood and J.-B. Baek, *Nature Communications*, 2020, **11**, 1278.
54. Y. Liu, X. Li, Q. Zhang, W. Li, Y. Xie, H. Liu, L. Shang, Z. Liu, Z. Chen, L. Gu, Z. Tang, T. Zhang and S. Lu, *Angewandte Chemie International Edition*, 2020, **59**, 1718-1726.
55. M. Zhang, J. Chen, H. Li, P. Cai, Y. Li and Z. Wen, *Nano Energy*, 2019, **61**, 576-583.
56. T. Qiu, Z. Liang, W. Guo, S. Gao, C. Qu, H. Tabassum, H. Zhang, B. Zhu, R. Zou and Y. Shao-Horn, *Nano Energy*, 2019, **58**, 1-10.
57. Q. Song, X. Qiao, L. Liu, Z. Xue, C. Huang and T. Wang, *Chem. Commun.*, 2019, **55**, 965-968.
58. H. Chen, X. Ai, W. Liu, Z. Xie, W. Feng, W. Chen and X. Zou, *Angew. Chem. Int. Ed.*, 2019, **58**, 11409-11413.
59. Q. Yao, B. Huang, N. Zhang, M. Sun, Q. Shao and X. Huang, *Angew. Chem. Int. Ed.*, 2019, **58**, 13983-13988.
60. W. Wu, Y. Wu, D. Zheng, K. Wang and Z. Tang, *Electrochim. Acta*, 2019, **320**, 134568.
61. E. Demir, S. Akbayrak, A. M. Önal and S. Özkar, *ACS Applied Materials & Interfaces*, 2018, **10**, 6299-6308.
62. H.-S. Park, J. Yang, M. K. Cho, Y. Lee, S. Cho, S.-D. Yim, B.-S. Kim, J. H. Jang and H.-K. Song, *Nano Energy*, 2019, **55**, 49-58.

63. F. Li, G.-F. Han, H.-J. Noh, I. Ahmad, I.-Y. Jeon and J.-B. Baek, *Adv. Mater.*, 2018, **30**, 1803676.
64. Z. Zhuang, Y. Wang, C.-Q. Xu, S. Liu, C. Chen, Q. Peng, Z. Zhuang, H. Xiao, Y. Pan, S. Lu, R. Yu, W.-C. Cheong, X. Cao, K. Wu, K. Sun, Y. Wang, D. Wang, J. Li and Y. Li, *Nat. Commun.*, 2019, **10**, 4875.
65. T. Liu, S. Wang, Q. Zhang, L. Chen, W. Hu and C. M. Li, *Chemical Communications*, 2018, **54**, 3343-3346.
66. Z. Li, Y. Feng, Y.-L. Liang, C.-Q. Cheng, C.-K. Dong, H. Liu and X.-W. Du, *Adv. Mater.*, 2020, **32**, 1908521.
67. J. Peng, Y. Chen, K. Wang, Z. Tang and S. Chen, *International Journal of Hydrogen Energy*, 2020, **45**, 18840-18849.
68. J. Duan, S. Chen, C. A. Ortíz-Ledón, M. Jaroniec and S.-Z. Qiao, *Angew. Chem. Int. Ed.*, 2020, **59**, 8181-8186.
69. L. Fu, Y. Li, N. Yao, F. Yang, G. Cheng and W. Luo, *ACS Catal.*, 2020, **10**, 7322-7327.
70. J. Lai, B. Huang, Y. Chao, X. Chen and S. Guo, *Adv. Mater.*, 2019, **31**, 1805541.
71. C.-H. Chen, D. Wu, Z. Li, R. Zhang, C.-G. Kuai, X.-R. Zhao, C.-K. Dong, S.-Z. Qiao, H. Liu and X.-W. Du, *Adv. Energy Mater.*, 2019, **9**, 1803913.
72. X. Wang, L. Bai, J. Lu, X. Zhang, D. Liu, H. Yang, J. Wang, P. K. Chu, S. Ramakrishna and X.-F. Yu, *Angew. Chem. Int. Ed.*, 2019, **58**, 19060-19066.
73. B. Wang, H. Huang, T. Sun, P. Yan, T. T. Isimjan, J. Tian and X. Yang, *Journal of Colloid and Interface Science*, 2020, **567**, 339-346.
74. Y. Zhao, H. Cong, P. Li, D. Wu, S. Chen and W. Luo, *Angew. Chem. Int. Ed.*, 2021, **60**, 7013-7017.
75. X. F. Lu, L. Yu, J. Zhang and X. W. Lou, *Adv. Mater.*, 2019, **31**, 1900699.
76. W. Liu, J. Ji, X. Yan, W. Liu, Y.-C. Huang, K. Wang, P. Jin, X. Yao and J. Jiang, *J. Mater. Chem. A*, 2020, **8**, 5255-5262.
77. H.-Y. Chen, H.-J. Niu, Z. Han, J.-J. Feng, H. Huang and A.-J. Wang, *Journal of Colloid and Interface Science*, 2020, **570**, 205-211.
78. Q. Wu, M. Luo, J. Han, W. Peng, Y. Zhao, D. Chen, M. Peng, J. Liu, F. M. F. de Groot and Y. Tan, *ACS Energy Letters*, 2020, **5**, 192-199.
79. W. Li, Z. Wei, B. Wang, Y. Liu, H. Song, Z. Tang, B. Yang and S. Lu, *Materials Chemistry Frontiers*, 2020, **4**, 277-284.
80. G. Liu, W. Zhou, B. Chen, Q. Zhang, X. Cui, B. Li, Z. Lai, Y. Chen, Z. Zhang, L. Gu and H. Zhang, *Nano Energy*, 2019, **66**, 104173.
81. Z. Liu, X. Yang, G. Hu and L. Feng, *ACS Sustain. Chem. Eng.*, 2020, **8**, 9136-9144.
82. B. You, N. Jiang, M. Sheng, S. Gul, J. Yano and Y. Sun, *Chem. Mater.*, 2015, **27**, 7636-7642.
83. J.-Q. Chi, W.-K. Gao, J.-H. Lin, B. Dong, K.-L. Yan, J.-F. Qin, B. Liu, Y.-M. Chai and C.-G. Liu, *ChemSusChem*, 2018, **11**, 743-752.
84. H. Yin, S. Zhao, K. Zhao, A. Muqsit, H. Tang, L. Chang, H. Zhao, Y. Gao and Z. Tang, *Nat. Commun.*, 2015, **6**, 6430.
85. Y. Li, L. A. Zhang, Y. Qin, F. Chu, Y. Kong, Y. Tao, Y. Li, Y. Bu, D. Ding and M. Liu, *ACS Catal.*, 2018, **8**, 5714-5720.
86. Z. Xing, C. Han, D. Wang, Q. Li and X. Yang, *ACS Catal.*, 2017, **7**, 7131-7135.

87. J. Liu, Y. Zheng, D. Zhu, A. Vasileff, T. Ling and S.-Z. Qiao, *Nanoscale*, 2017, **9**, 16616-16621.
88. S. Anantharaj, K. Karthick, M. Venkatesh, T. V. S. V. Simha, A. S. Salunke, L. Ma, H. Liang and S. Kundu, *Nano Energy*, 2017, **39**, 30-43.
89. L. Guo, F. Luo, F. Guo, Q. Zhang, K. Qu, Z. Yang and W. Cai, *Chem. Commun.*, 2019, **55**, 7623-7626.
90. L. Tang, J. Yu, Y. Zhang, Z. Tang and Y. Qin, *RSC Adv.*, 2021, **11**, 6107-6113.
91. B. Lu, L. Guo, F. Wu, Y. Peng, J. E. Lu, T. J. Smart, N. Wang, Y. Z. Finfrock, D. Morris, P. Zhang, N. Li, P. Gao, Y. Ping and S. Chen, *Nature Communications*, 2019, **10**, 631.
92. H. Wang, C. Xu, Q. Chen, M. Ming, Y. Wang, T. Sun, Y. Zhang, D. Gao, J. Bi and G. Fan, *ACS Sustain. Chem. Eng.*, 2019, **7**, 1178-1184.
93. Z.-L. Wang, K. Sun, J. Henzie, X. Hao, C. Li, T. Takei, Y.-M. Kang and Y. Yamauchi, *Angewandte Chemie International Edition*, 2018, **57**, 5848-5852.
94. J. Wang, Z. Wei, S. Mao, H. Li and Y. Wang, *Energy Environ. Sci.*, 2018, **11**, 800-806.
95. J.-S. Li, M.-J. Huang, X.-N. Chen, L.-X. Kong, Y.-W. Zhou, M.-Y. Wang, J.-L. Li, Z.-X. Wu and X.-F. Xu, *Chemical Communications*, 2020, **56**, 6802-6805.